Determining a Lower Limit of Luminosity for the First Satellite Observation of a Reverse Beam Terrestrial Gamma-ray Flash Associated with a Cloud to Ground Lightning Leader

Jeffrey M. Chaffin[1,4], Yunjiao Pu[2], David M. Smith[1], Steve Cummer[2], Michael Splitt[3]

[1]University of California Santa Cruz, Santa Cruz, CA, USA
[2]Duke University, Durham, NC, USA
[3]Florida Institute of Technology, Melbourne, FL, USA
[4]Air Force Institute of Technology, WPAFB, OH, USA

Key Points:

- Using the timing alignment of multi-wavelength observations and estimates of thunderstorm charging altitudes we estimate the likely altitude of the TGF to be 7.5 km.
- The minimum luminosity estimate for a downward TGF at 7.5 km to be detected by Fermi/GBM via the reverse beam is 2×10^{18} photons above 1 MeV.
- We found the e-folding attenuation length in grammage for the reverse beam component of a TGF to be 58 g/cm^2.

Corresponding author: Jeffrey Chaffin, `Jeffrey.Chaffin.ctr@afit.edu`

Abstract

We provide an updated analysis of the gamma ray signature of a terrestrial gamma ray flash (TGF) detected by the Fermi Gamma-ray Burst Monitor first reported by Pu et al. (2020). A TGF produced 3 ms prior to a negative cloud-to-ground return stroke was close to simultaneous with an isolated low frequency radio pulse during the leader's propagation, with a polarity indicating downward moving negative charge. In previous observations this 'slow' low frequency signal has been strongly correlated with upward directed (opposite polarity) TGF events (Pu et al., 2019; Cummer et al., 2011), leading the authors to conclude that the Fermi gamma ray observation is actually the result of a reverse positron beam generating upward directed gamma rays. We investigate the feasibility of this scenario and determine a lower limit on the luminosity of the downward TGF from the perspective of gamma ray timing uncertainties, TGF Monte Carlo simulations, and meteorological analysis of a model storm cell and its possible charge structure altitudes. We determined that the most likely source altitude of the TGF reverse beam was 7.5 km $\pm$ 2.6 km, just below an estimated negative charge center at 8 km. At that altitude the Monte Carlo simulations indicate a lower luminosity limit of 2×10^{18} photons above 1 MeV for the main downward beam of the TGF, making the reverse beam detectable by the Fermi Gamma-ray Burst Monitor.

1 Introduction

It is widely accepted that terrestrial gamma ray flashes (TGFs) are the result of bremsstrahlung interactions of large populations of highly energetic electrons with atmospheric molecules. These relativistic electrons are driven by thunderstorm electric field activity consisting of a combination of the background electric field strength of the storm cell and enhancements to that field by transient electric fields associated with lightning leaders (J. Dwyer et al., 2012). The analysis of the first observations of TGFs (Fishman et al., 1994) misjudged the depth of the source altitude and consequently the intrinsic brightness was underestimated. It was initially proposed that the source altitude of TGFs must be high in the stratosphere connected with the runaway breakdown of sprites (Taranenko & Roussel-Dupré, 1996). Later, the analysis of the cumulative energy spectra of TGFs observed by the Reuven Ramaty High Energy Solar Spectroscopic Imager (RHESSI) lowered the source altitude estimate by at least 30 km. Using the relativistic runaway electron avalanche (RREA) model (Gurevich et al., 1992; Dwyer, 2003a), it was shown that the production altitudes of the RHESSI TGF observations were consistent with 15-21 km, conventional thunderstorm altitudes, and with intrinsic brightness estimates as high as 10^{17} gammas above 1 MeV (Dwyer & Smith, 2005). This analysis, along with work linking TGFs to the lightning discharge process (Cummer et al., 2005; Stanley et al., 2006; Lu et al., 2010; Cummer et al., 2014; Lindanger et al., 2021), confirmed that TGFs occur lower in Earth's atmosphere and at intensities much brighter than previously considered.

Ground observations of lightning-associated high energy radiation events need to be classified according to their spectral, temporal, and luminosity characteristics. For instance, low-luminosity events associated with lightning-stepped leaders have fast time profiles on the order of μs and lack higher energy counts above 1-2MeV (Moore et al., 2001; Dwyer et al., 2004b; J. Dwyer et al., 2005). On the other hand, ground observations of TGFs are characterized by broad time profiles 10s-100s of μs, high-energy counts in the 10s of MeV and luminosities equivalent to those of TGFs reported from space (Dwyer et al., 2004b; Tran et al., 2015; Hare et al., 2016; Bowers et al., 2017; Enoto et al., 2017; Abbasi et al., 2022; Wada et al., 2022; Kereszy et al., 2022). There are also ground-based observations that are referred to in the literature as TGFs that are lower in luminosity and 'spiky' in time profile similar to stepped-leader X-rays but with a harder spectrum, like those observed from space (Abbasi et al., 2017, 2018). With these characteristics in mind, we have seen that TGFs can occur at any altitude where thunderstorm charging and lightning initiation take place.

As a general statement, space based observations detect upward directed TGFs, while ground based observations are of downward directed TGFs. However, this does not rule out the possibility of TGF detection when observed from the opposite view point, e.g. detecting an upward directed TGF from the ground. High-energy gamma rays can generate positrons through pair production; and if produced while still within the avalanche region will run away in the opposite direction of the electrons (A. Gurevich et al., 2000). Runaway positrons, though smaller in number and unable to avalanche like their electron counterparts, will still produce their own gamma rays via bremsstrahlung (Dwyer, 2003a). This reverse beam component of the TGF has previously been observed by the Airborne Detector for Energetic Lightning Emissions (ADELE) when flying through the eye-wall of Hurricane Patricia aboard the National Oceanic and Atmospheric Administration's Hurricane Hunter WP-3D Orion (Bowers et al., 2018). Modeling work by Ortberg et al. (2020) suggests that upward TGFs observable from space can theoretically be co-observed from the ground if the ground observation point is at sufficient altitude, say a mountaintop.

But what about detecting a downward TGF from orbit? Pu et al. (2020) published a Fermi TGF that took place at 02:23:12.82895 UT on 25 July 2019. It consisted of eight counts in the two bismuth germanate (BGO) detectors. The BGO detectors have an energy range of 200 keV to 40 MeV and a combined effective area of 322 cm^2. They found that the TGF was unambiguously associated with a negative CG lightning flash, i.e. a lightning leader with a polarity that would move negative charge towards the ground. They arrived at this conclusion using observational data from the Fermi Gamma-ray Burst Monitor (GBM) and simultaneous ground-based radio measurements of lightning from a network of very low frequency (VLF) and low frequency (LF) magnetic sensors run by Duke University.

Research done in the last decade has shown a relationship between TGFs and several types of low-frequency radio emissions from lightning (Cummer et al., 2011; Lyu et al., 2015, 2016, 2021; Pu et al., 2019). Of these unique radio pulses simultaneous to TGF production, the "slow pulse" (Cummer et al., 2011) is characterized by a distinct slow temporal signature (50-100 μs). The pulse comes in the midst of initial breakdown pulses (IBPs), which are typically less than 10 μs in duration. Dwyer and Cummer (2013) demonstrated how this slow pulse can be interpreted as an observable current moment of the TGF electron avalanche process itself. The Fermi TGF in question (Pu et al., 2020) was simultaneous to a distinct slow pulse (120 μs) that is consistent with slow low-frequency pulses that have previously been associated with TGFs produced by IC leaders (Cummer et al., 2011; Østgaard et al., 2013; Pu et al., 2019). The authors make clear that the polarity of this slow pulse is opposite to that for upward TGFs produced by IC leaders and is the same as that for a downward TGF produced by a rocket-triggered upward positive leader (Hare et al., 2016). The conclusion drawn is that the TGF must be directed downwards and the Fermi observation is consequently of the reverse beam (positron initiated) gamma-rays.

Using a timing alignment procedure detailed in Pu et al. (2019) and location data from the National Lightning Detection Network (NLDN), Pu et al. (2020) determined the source altitude for the TGF to be from 5.4-6.7 km. The slow-pulse event occurs roughly 3 ms after the initial breakdown pulses signaling the initiation of the downward negative leader, and roughly 3 ms prior to the return stroke. Assuming a leader propagation speed of 10^6 m/s (Zhu et al., 2016) this puts the initiation altitude of the leader nominally at 6 km, leading the authors to argue a scenario in which the TGF was produced ahead of the positive polarity end of a bidirectional CG leader. Such a scenario does lend support for the TGF to be unusually bright. A recent modeling paper by Dwyer (2021) found that for a downward TGF produced at the tip of a positive leader the gamma ray burst can be much more intense than those produced at the tips of negative leaders.

Considering that a TGF would experience considerable absorption from a source altitude of 6 km, and that the reverse beam TGF is understood to be roughly 1% the brightness of the main forward beam (Ortberg et al., 2020) is this observation under these

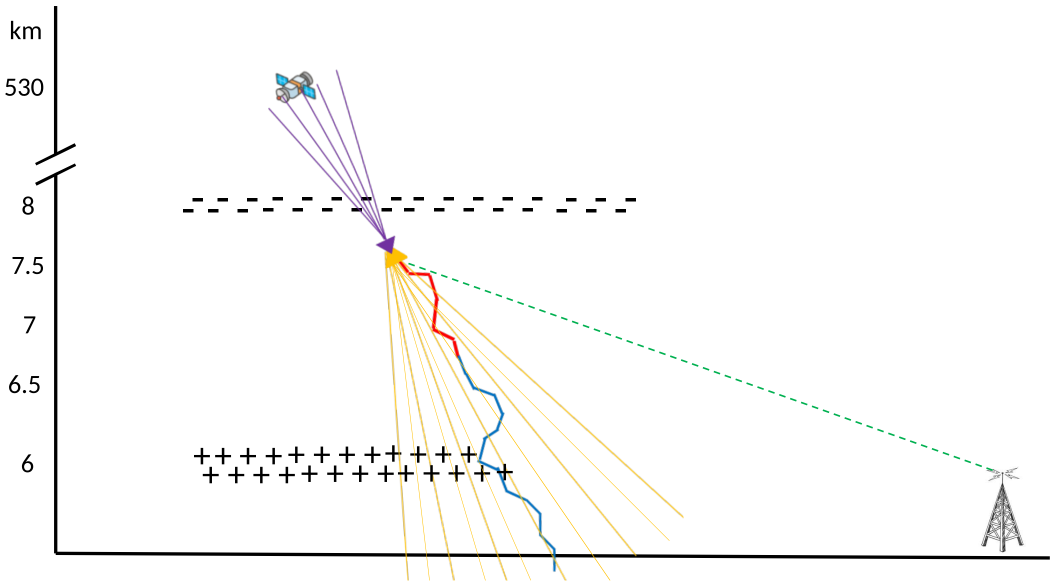

Figure 1. Qualitative depiction of the proposed TGF scenario. Altitude values are determined by the methods in Sections 3 and 4. The model storm cell analysis estimates a negative charge center at 8 km and a positive charge center at 6 km. A bi-directional CG leader initiates at roughly 6-7 km. The negative-polarity leader (blue) propagates towards ground resulting in a return stroke 6 ms later. The positive-polarity end of the leader (red) propagates upward, initiating a downward TGF (yellow) 3 ms after leader initiation at roughly 7.5 km, just below the negative charge center. The resulting TGF beaming angle is such that the reverse beam (purple) is closely aligned (within a 50 km annulus) with the Fermi/GBM satellite. Fermi/GBM observes a small count rate TGF (purple) produced simultaneous to the resulting radio sferic observation (green) created by the current moment associated with the electron avalanche (RREA) responsible for the TGF.

circumstances possible? Can a reverse beam TGF be seen from space from so deep in the atmosphere, and how bright would the main (downward) TGF need to be? In this paper we use Monte Carlo simulations to estimate the brightness required for a reverse beam TGF to be observed at orbital altitudes. We will attempt to further constrain the likely source altitude using a charge structure analysis of the storm cell and provide a new source altitude estimate with updated timing alignment analysis.

2 Refined Altitude Estimate

The altitude estimate is derived from the relative timing of radio and gamma-ray signals. In Pu et al. (2020) the only source of uncertainty was the uncertainty in the NLDN position. Here, we summarize the timing alignment analysis and associated error and propose a more likely source altitude for the TGF. We will also introduce additional terms of uncertainty due to both an unaccounted for positive leader propagation and the limited statistics of the gamma-ray signal.

The timing alignment method demonstrated by Pu et al. (2019) used the assumed simultaneity between the TGF electron avalanche and subsequent gamma-ray observations with the slow-pulse observed in the LF and VLF sensors. Using the two-dimensional (geographic) NLDN location the arrival times of each signal were corrected for time of flight and the time difference between the centroids of each was determined. The altitude that minimized this time difference gave the best estimate for the TGF source altitude. The quoted uncertainty in the analysis of Pu et al. (2020) came from the NLDN error ellipse, which surrounds the best location of the lightning event. The ellipse represents the 95% confidence interval of the triangulated location using the NLDN LF sensor suite. Locations along the perimeter of the ellipse are used to determine a minimized delta time between arrival times by adjusting the altitude up or down from the source altitude derived from the NLDN location. As you move around the ellipse there is one location that requires the altitude estimate to be moved up the most and one location that requires it to be moved down the most. In this way you get a range of altitude error for the particular NLDN location and altitude estimate. This alignment procedure was done for the reverse beam observation published in Pu et al. (2020) and is the justification for the 6±0.4 km TGF source altitude estimate.

The original analysis uses the NLDN location for the return stroke of the -CG event. As described in Pu et al. (2020) the slow pulse occurs 3 ms prior to the return stroke with the initial breakdown pulses (IBP) occurring 3 ms prior to that. Using a typical -CG leader progression speed of 10^6 m/s and a time from the IBPs to the return stroke of roughly 6 ms, the negative leader tip would have been at an altitude of 3 km when the Fermi reported TGF occurred. Considering that the leader tip would further travel less than 1 km from the ground when the return stroke occurred Pu et al. (2020) argues that the most likely scenario is that the TGF was produced nearer to the initiation point, possibly associated with the positive polarity end of a bidirectional CG leader. See Figure 1 for a qualitative description of our proposed scenario. NLDN recorded a signal at 02:23:12.824 UT on 25 July 2019. This signal is roughly 6 ms prior to the return stroke signal with a significantly smaller peak current and horizontal distance of 1.7 km from the return stroke. We believe this signal to be the initial breakdown pulses (IBPs) of a single lightning event. The NLDN location is given as 26.6378 latitude and -77.2002 longitude. This is our best estimate for the location of the TGF though the positive polarity leader may have traveled some distance horizontally from this location within the 3 ms time difference between the IBPs and TGF. Redoing the timing alignment analysis described earlier with this new location results in an estimated source altitude of 7.5km with an error of ±0.75 km derived from the NLDN error ellipse described previously.

It is important however to account for the possible horizontal propagation of the positive leader in the 3ms between the IBPs and the slow pulse/TGF signals. If we take the extreme case that the positive leader traveled purely horizontally during those 3 ms and use a propagation speed of 10^5 m/s (Biagi et al., 2011; Wang et al., 2016; Kotovsky et al., 2019), then the maximum horizontal distance the positive leader could have traveled from the NLDN IBP location would be 300 meters. We can again make use of the assumption of simultaneity between the arrival times of the gamma rays and the slow pulse signal to determine the extent a horizontal shift of 300 meters would make to the source altitude estimate. We draw a circle around the NLDN location of radius 300 meters. At each point on that circle the source altitude would need to be adjusted to keep the arrival time difference of the two signals near zero. Similarly to the NLDN error ellipse, as you move around the circle, there is one location on the circumference that requires the altitude to be moved up from 7.5km to a maximum and one point that requires it to be moved down to a minimum. The maximum altitude to maintain signal simultaneity for a point 300 meters from the NLDN location is 7.77 km and the minimum altitude is 7.15 km, giving a source altitude error of ±0.31 km.

Lastly, there is an uncertainty in the gamma ray arrival times at the Fermi/GBM that was not taken into account in the original analysis. The 8 counts incident on the BGO detectors should be considered a random sample from an unknown parent distribution, the mean of which will vary with respect to the sample mean. Assuming a Gaussian parent distribution, the standard deviation of the mean (centroid) of the BGO counts is the standard deviation s of the sample population divided by the square root of the number of counts N in the sample population or $\frac{s}{\sqrt{N}}$. The error in the centroid of the arrival times of the gamma rays is ± 8.2 μs. This timing uncertainty Δt can be converted into an altitude uncertainty Δh. The propagation time of the gamma ray signal is defined as

$$t = \frac{L}{c}$$

where L is the distance between the TGF source and Fermi as a function of h, the assumed altitude of the TGF.

$$t = \sqrt{(116km)^2 + (530km - h)^2}/c$$

The horizontal offset between the NLDN location and the nadir of Fermi is 116 km. The altitude of Fermi is 530 km. By taking the derivative of t with respect to h, we can solve for the error in h,

$$\Delta h = \Delta t(c\sqrt{(116km)^2 + (530km - h)^2})/(530km - h)$$

where Δt is the standard deviation of the mean of the GBM signal (8.2 μs). When h=7.5 km the calculation results in an uncertainty in the altitude of the source, from the uncertainty in the arrival times of the gamma rays, of ± 2.5 km. When we add the three uncertainties in quadrature,

$$\Delta h_{total} = \sqrt{\Delta h^2_{NLDN} + \Delta h^2_{positiveleader} + \Delta h^2_{gamma}}$$

we get an error in our altitude estimate of 7.5 ±2.63 km, with the gamma ray timing uncertainty dominating.

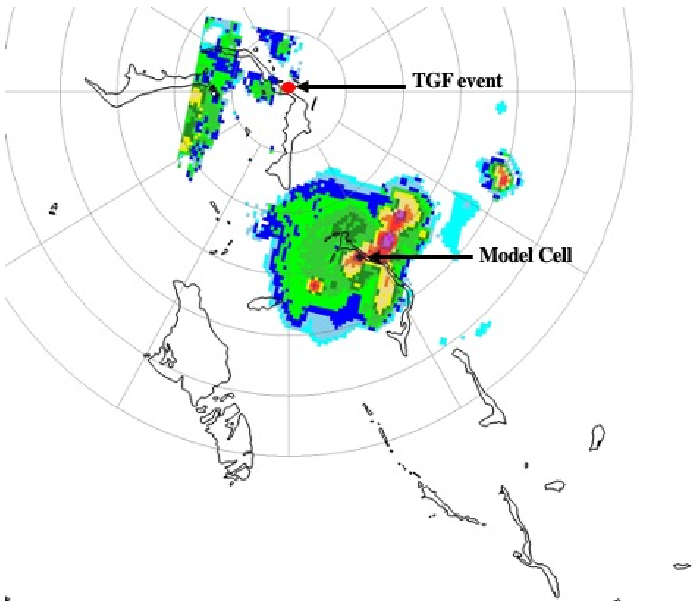

Figure 2. Composite reflectivity of the HRRR model over the Bahamas Islands at 02:00:00 UT (roughly 23 minutes prior to the TGF). Range rings in 50 km increments are centered at the July 25 event (26.6378,-77.2002). Our chosen model cell is close to land, similar to the TGF location, but near an adjacent island.

3 Meteorology

To determine whether the source altitude estimate derived in Section 2 is consistent with where we might expect the charge centers of the storm cell to be, we use the High-Resolution Rapid Refresh (HRRR) model (Dowell et al., 2022) of a nearby storm cell. The HRRR model is a convection-allowing numerical model with hourly data assimilation that covers the conterminous United States and runs in real time at the NOAA/National

Centers for Environmental Prediction (NCEP). HRRR initialization is designed for optimal short-range forecasting skills with a particular focus on the evolution of precipitating systems. The model forecast includes many atmospheric variables, including those of hydrometeor types and quantities, which are relevant for discussions of cloud charging in convective systems. Note that while weather radar data are used to help initialize this model, it is unclear whether they would have had the Bahamas radar for inclusion. As the data assimilation is hourly, meaning that we only have model data on the hour, e.g. 0200, 0300 etc., we use model data for the closest storm cell of equivalent evolution for the hour nearest to the TGF event. The TGF event was observed by Fermi at 02:23:12.82895 UT on 25 July 2019. The modeled storm cell was located 150 km from and just prior (02:00:00 UT) to the July 25 event. In Figure 2 you can see that the model cell is close to land, similar to the TGF location, but close to an adjacent island. Figure 3 shows a scatter plot of all NLDN lightning event peak currents that occurred within 20 minutes and 10 km of the event associated with the TGF (red). NLDN events are identified as either CG (black) or IC (blue). There is a clear dominance of -CG events during this period, suggesting a tripole charge structure where the lower positive charge center is relatively weak or nonexistent.

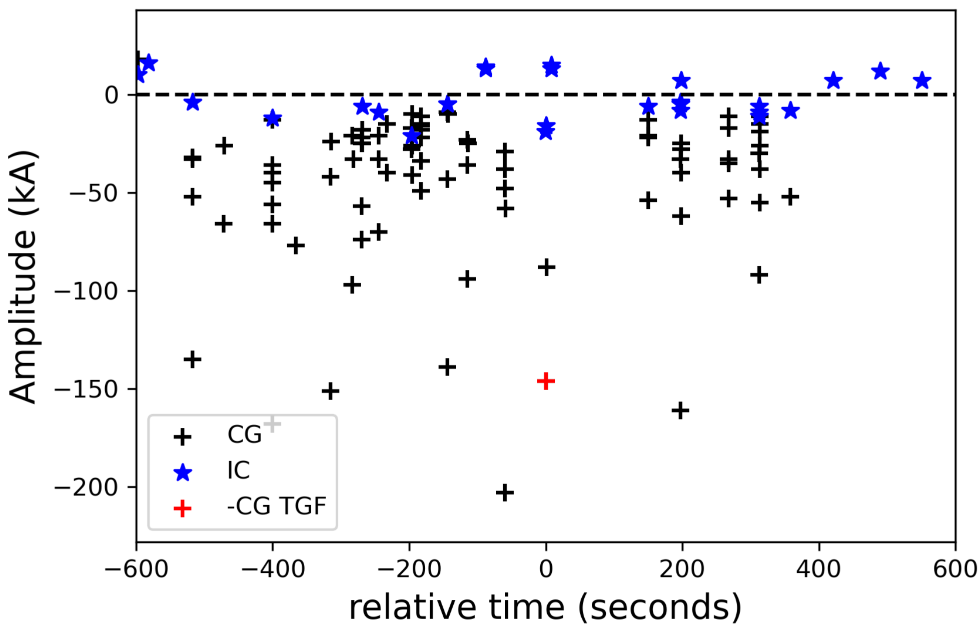

Figure 3. Peak current of all NLDN lightning events (CG in black +. IC in blue ⋆) within 20 minutes and 10 km of the -CG flash associated with the TGF (red +).

Hydrometeor mixing ratios were used to assess non-inductive charging of the model cell as a function of cloud water content, ice crystal content, graupel content and temperature (Takahashi, 1978; Jayaratne, 1983). When ice crystals collide with graupel in the presence of supercooled water droplets, charge is transferred between these ice particles so that they are left with either a surplus or deficit of electrons following the collision. The vertical profile of the 02:00:00 UT model cell is plotted in Figure 4. The altitude range between 6 km and 8 km is where liquid water content (purple), graupel (red), and ice crystals (green) are substantially present and non-inductive charging would be expected. The direction of charge exchange is heavily dependent on temperature and water content. Luque et al. (2020) shows that the temperature at which charge exchange

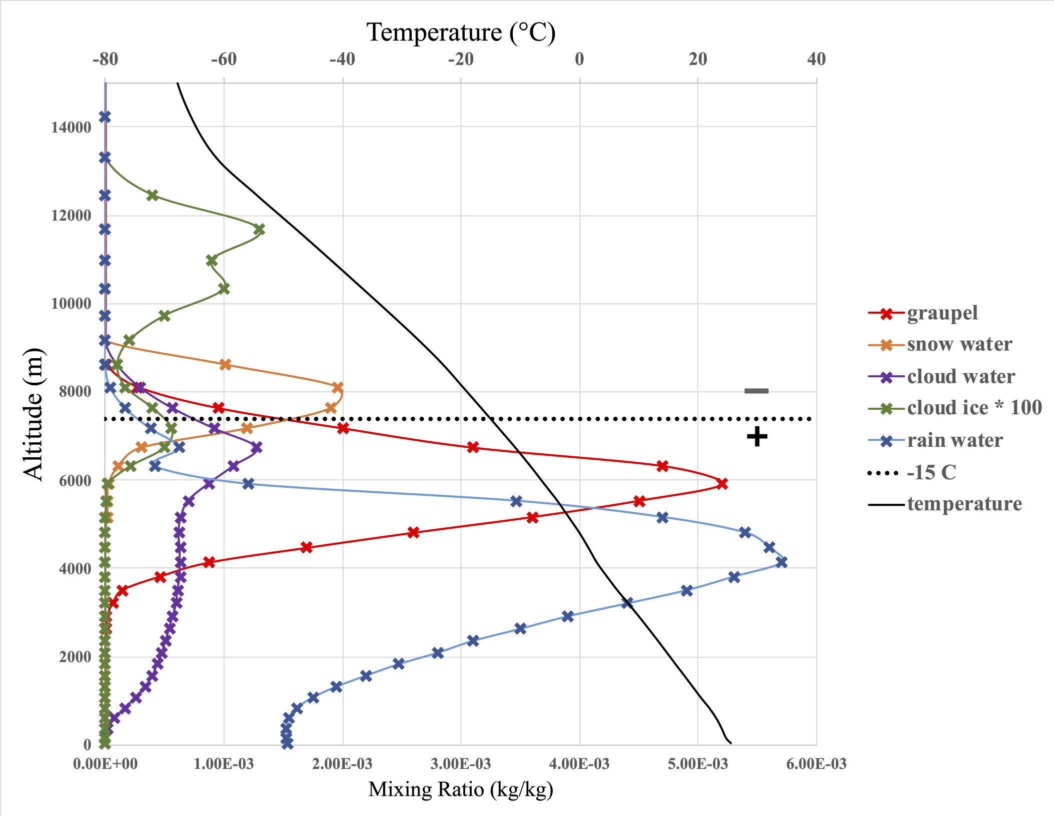

Figure 4. Mixing ratios are plotted with respect to altitude, with graupel in red, snow in orange, cloud water in purple, cloud ice in green but multiplied by 100 to be visible on plot, and rain water in blue. Air temperature as a function of altitude is plotted in black. The altitude range with highest percentages of cloud water content (Purple), ice crystals (green) and graupel (red) is between 6 km and 8 km denoting the likely range of maximum charge separation. The -15°C 'reversal temperature' (dotted black line)is just above 7000 m with positive charging occurring below this altitude and negative charging above.

reverses is -15C. Below the -15C reversal temperature and where graupel (red) has its peak around 6 km there is a high probability for positive charging (positively charged graupel). Above the -15C temperature altitude where the snow mixture (orange) peaks at 8 km, there are strong indications for negative charging. Considering that the model storm cell was part of the same weather system, close in time, location, and similar in terms of the development stage to the cell that produced the TGF the model values are considered fairly representative and indicate that the TGF producing cell developed an electric field roughly between 6 and 8 km directed upward, consistent with a bi-directional CG leader moving negative charge downward. Though the source altitude uncertainty from Section 2 extends up to 10 km, the charging analysis suggests that TGF source altitude estimates above 8 km become less likely as electron avalanches in that altitude range would be directed upward away from the negative charge center and toward an upper positive, which would be a scenario unsupported by the Duke University radio data.

4 Monte Carlo Simulations

To determine a lower limit of TGF luminosity, we performed several Monte Carlo simulations using Geant4 (Agostinelli et al., 2003; Allison et al., 2006, 2016). Assuming an RREA production mechanism we compared the number of photons incident on the two Fermi/GBM bismuth germanate (BGO) detectors, as published in Pu et al. (2020), to the simulated gamma ray fluence from the reverse beam component of a downward directed TGF. Our GEANT4 atmospheric simulation consists of stacked cylindrical slabs, 2000 km in radius and each 0.5 km in height. Each slab was filled with an atmosphere that depended on the characteristic temperature, pressure, and density of its midpoint. The temperature, pressure, and density values were sourced from the U.S. Standard Atmosphere (1976). In each simulation, a photon distribution was released and propagated upward through the mass model of the atmosphere. A boundary was set at 530 km such that all particles passing the boundary with a positive (upward) Z-axis momentum were noted. As a result, the radiation field generated at an orbital altitude of 530 km was recorded. We performed simulations for various TGF source altitudes by inputting the photon distribution at altitudes from 6 km to 12 km. The entire simulation code is included in the public data release.

The input photon distribution comes from TGF simulations using the relativistic electron avalanche model (REAM) discussed in Dwyer (2003a); Dwyer (2007) and Dwyer and Smith (2005). The REAM simulation is initiated by injecting a single high-energy seed electron into the top of a high field region of -400 kV/m. The seed electron represents a possible knock-off electron produced by a cosmic-ray muon. This results in an exponential increase in relativistic electrons or relativistic electron avalanches. The energy distribution of the electrons can be approximated by the exponential $e^{-E/7.3MeV}$ (J. Dwyer et al., 2012). The subsequent bremsstrahlung gamma rays from electron and positron interactions with atmospheric molecules are tracked and recorded with energy, position, and direction information. Photons with z-component momentum aligned with the electric field direction, i.e. the reverse beam, are used as the input photon distribution in the previously mentioned atmospheric simulation.

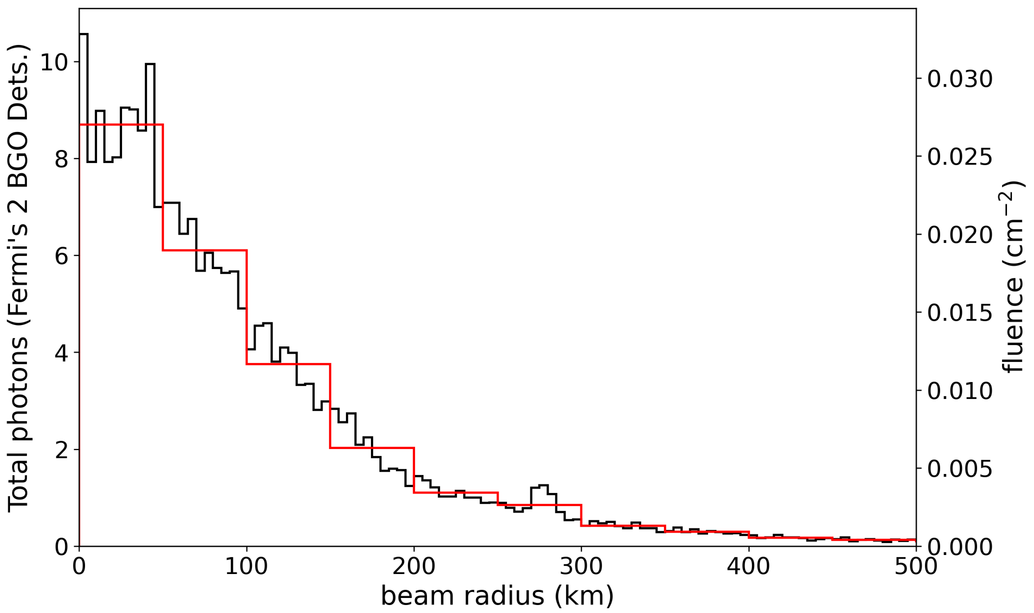

Figure 5. Black: Reverse beam gamma ray fluence of an 8 km source altitude TGF simulation scaled to a 1.5×10^{18} main beam intensity binned in 5 km wide annuli. Red: Same, binned in 50km wide annuli. Right vertical axis is fluence in counts per cm^2. Left vertical axis is the total counts expected in both BGO detectors combined using a total effective area of 322 cm^2.

TGF luminosity observed from orbit will depend on the degree of horizontal offset between the spacecraft and the center of the beam. The horizontal distance between the NLDN location and the Fermi/GBM is approximately 116 km (Pu et al., 2020). To estimate the minimum required intrinsic luminosity we will assume an optimally favorable tilt of the TGF such that the Fermi satellite falls within a 50 km radius of the reverse TGF beam center. Within 50 km from the beam center, the simulated fluence was relatively constant and began to fall off outside of the 50 km radius. Figure 5 shows the simulated reverse beam gamma ray fluence of an 8 km source altitude TGF scaled to a 1.5×10^{18} gamma rays >1MeV main beam intensity binned in 5 km and 50 km wide annuli.

Pu et al. (2020) notes that only the counts of the two BGO detectors of the Fermi/GBM were used in the timing alignment procedure. For a TGF-like spectrum, the effective area of the BGO detectors is 161 cm^2 (Tierney et al., 2013). Multiplying the effective area by the fluence and limiting the calculated fluence to photons greater than the lower limit of the BGO detectors (200 keV) (Briggs et al., 2013), we derive the probable number of simulated photons recorded by each detector.

5 Simulation Results

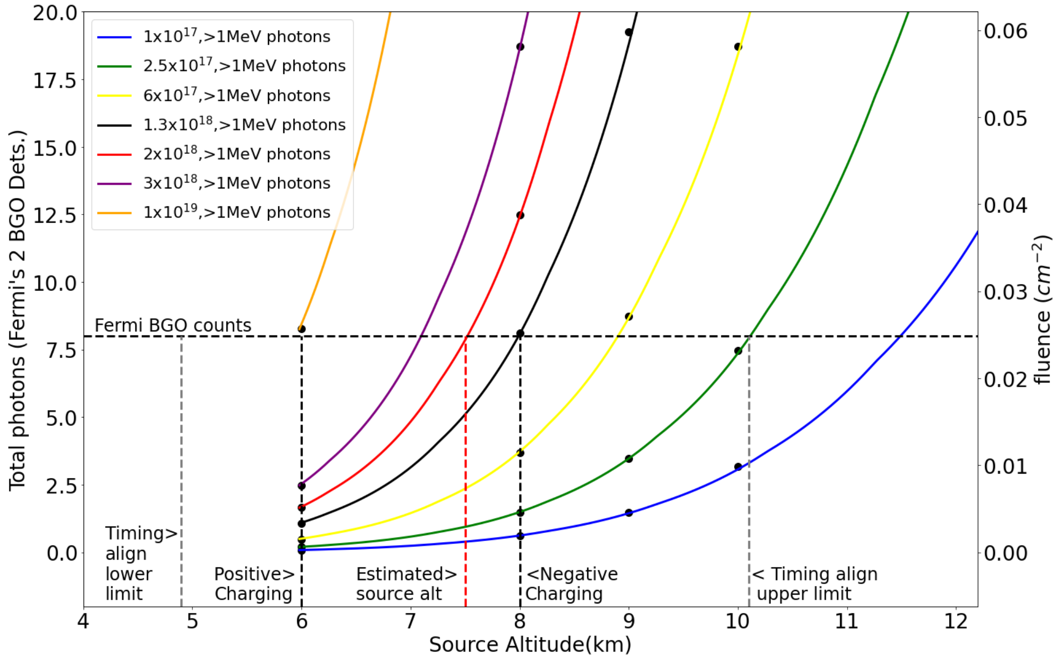

Figure 6. Data points represent the averaged simulated reverse beam fluence within a disk of radius 50 km from beam center captured at an orbital altitude of 530 km. A curve is fit to data points of the same intrinsic brightness. The horizontal dashed line indicates the number of counts incident on the two Fermi/BGO detectors of the July 25 event. The vertical dashed red line indicates the source altitude estimate of 7.5 km, as derived in Section 2, and the uncertainty in that estimate is marked by the two vertical grey dashed lines. The two vertical black dashed lines indicate the likely positive and negative charge center altitudes discussed in Section 3.

The results of the Geant4 Monte Carlo simulations are presented in Figure 6. Each data point represents the averaged simulated reverse beam fluence (right vertical axis) within a 50 km radial disk from beam center at 530 km as a function of source altitude and intrinsic brightness of the main (downward) beam. The left vertical axis shows the expected number of photons incident on Fermi's two BGO detectors by multiplying the combined effective area (322 cm^2) by the fluence on the right. A curve is fit to data points of the same source luminosity. The fitting was done using column density in g/cm^2 with the exponential model $F = F_0 e^{-\mu g}$, where F_0 is the fluence if there was no atmosphere between the TGF source and Fermi, and μ is a mass absorption coefficient of 0.0173 cm^2/g for all curves. The x-axis has been translated from column density to altitude in km for easier comparison of altitude estimates. The vertical dashed red line indicates the source altitude estimate of 7.5 km as derived in Section 2. We discussed in Section 3 that even though the altitude uncertainty (vertical grey dashed lines) is quite broad on account of the gamma ray arrival time uncertainty, the storm cell charge structure analysis limits the source altitude to below 8 km. A TGF at 7.5 km is consistent with the HRRR analysis, locating the TGF just below the altitude estimate of negative charging in the model storm cell. This supports the scenario of a positive polarity leader propagating upward towards a negative charge center, resulting in a TGF (Dwyer et al., 2004a; Hare et al., 2016; Smith et al., 2018). You can see in Figure 6 (where the red curve and the vertical dashed red line intersect) that at an estimated source altitude of 7.5 km, the lower limit of intrinsic brightness of the TGF, consistent with the minimum fluence required for a Fermi/GBM detection (8 counts), is 2×10^{18}.

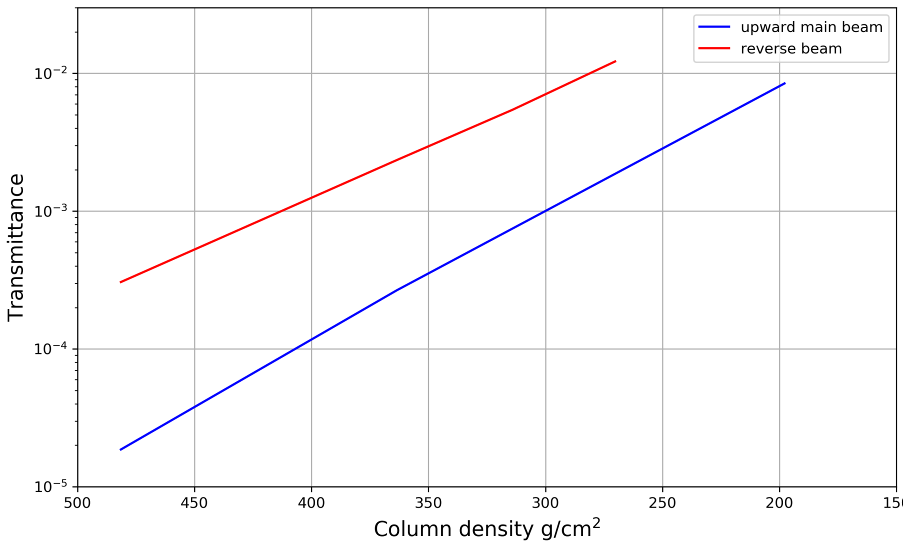

Figure 7. Transmittance (between 0-1) as a function of column density (g/cm^2) for both upward directed main beam TGF simulations (blue) and upward directed reverse beam TGF simulations (red). The transmittance was calculated using input photons with energies greater than 1 MeV and captured output photons with energies greater than 200 keV at 530 km.

6 Discussion

Is this brightness estimate reasonable? There are several examples in the literature of TGFs with luminosities of orders of magnitude similar to our estimate of 2×10^{18} (Mailyan et al., 2016; Smith et al., 2020). In particular, we refer to a TGF over the Mediterranean basin estimated to be as bright as 3×10^{18} photons with energy >1 MeV (Gjesteland et al., 2015). The distribution of TGF intensities has been shown to be consistent with a power law of index of -2.2 to -2.4, using RHESSI and Fermi together (Østgaard et al., 2012), Fermi alone (Tierney et al., 2013), and AGILE (Marisaldi et al., 2014). We can use this index to estimate how rare a bright TGF such as the Mediterranean event is. Dwyer et al. (2017) defines a standard TGF luminosity of 3×10^{16}. We'll use this luminosity value as an approximation for the minimum detectable Fermi TGF. By taking the ratio of the integral of $x^{-2.3}$ from 3×10^{16} to infinity and from 3×10^{18} to infinity we get a result of roughly one bright Mediterranean-like event in 400 or on the order of 10 events in the orbital TGF catalog. In addition, our brightness estimate assumes an optimal beaming angle. The actual angular offset between Fermi and the vertical of the source position is only 12.5°. With an angular band corresponding to the inner 50 km annulus of approximately 5.5° the TGF would only need to be offset from vertical by 7° to be optimally beamed. With an average angular offset of roughly 30° between Fermi and the Fermi catalog of TGF source locations, it makes sense that the first known orbital observation of a reverse beam TGF is one where optimal beaming is likely and the intensity of the event falls within the upper end of the TGF luminosity distribution.

We initially thought that it would be impossible for a TGF that was deeper in the atmosphere than any previous orbital observation, and was considered to be the reverse beam component of the TGF, to be observed at orbital altitudes. As a check on the results of our simulation, we present two lines of argument. First, in Figure 7 we have plotted the transmittance as a function of column density, in g/cm^2, for both an upward-directed TGF main beam and an upward-directed reverse beam. Transmittance is a measure of probability. In this instance, it is the probability of a photon from either a TGF main beam or reverse beam to penetrate the atmosphere and escape to orbital altitudes. The larger the transmittance, the greater the probability that photons will escape. Transmittance was calculated using the ratio of captured output photons of energies greater than 200 keV at 530 km to the REAM input photons of energies greater than 1 MeV. All simulations were performed using the same Geant4 atmospheric simulation code discussed in Section 4. You can see in Figure 7 for a TGF that is sourced at any point between 6 km and 8 km (481 g/cm^2 and 363 g/cm^2 respectively), the reverse beam transmittance is roughly an order of magnitude larger than the main beam. This is consistent with our understanding of a reverse beam spectrum. Although the reverse beam ratio to the forward beam is only 0.78% for photons greater than 1 MeV, it is higher in average energy making it more penetrating or likely to escape. (Bowers et al., 2018; Ortberg et al., 2020). For electron initiated bremsstrahlung most of the electrons are produced in the last e-folding of the avalanche, i.e. they carry only a small fraction of the total potential of the thunderstorm. Positrons do not avalanche, because a positron can not knock another positron out of an atom. Therefore, the positrons traveled on average about half the total potential of the storm instead of just the last bit of it. So, they have an average energy higher than that of the electrons, although there are far fewer of them. This difference in the hardness of the spectrum between the forward and reverse beams is made more apparent when we calculate the average e-folding attenuation length of each. For our upward-directed main beam TGF simulations we found an e-folding attenuation length of 46 g/cm^2 which is consistent with the Smith et al. (2010) estimation of 45 g/cm^2. The reverse beam simulations resulted in an average e-folding attenuation length of 58 g/cm^2 calculated for depths ranging from 270 g/cm^2 (10km altitude) to 481 g/cm^2 (6km altitude) of overlying air.

Let us assume that the reverse beam fluence at 530 km is evenly distributed over a disk of 120km radius, which corresponds to the 12.5° angular offset between the reported TGF/lightning location and Fermi. Thus, the photons are distributed in an area 4.57×10^{14} cm^2. This isn't an unreasonable order of magnitude estimate as our simulations show that 80% of the reverse beam fluence is within 150 km of beam center and previous simulation work has also shown the reverse beam is inherently more narrowly beamed (Bowers et al., 2018; Ortberg et al., 2020). This calculation was made by taking the ratio of the total simulated fluence at 530 km out to 150 km along the horizontal projection to the total fluence at 530 km out to 2000 km along the horizontal projection. This result is noteworthy in that along with having a larger transmittance, the beam is more concentrated, both of which increase the detection probability.

Let's also assume a TGF main beam source luminosity of 10^{17} photons > 1MeV, a transmittance (from Figure 7) for an 8km (363.54g/cm^2) reverse beam of 2.35×10^{-3}, and a factor of 0.78% for the reverse beam ratio of luminosity to the main beam. Using these values, the fluence of the reverse beam can be estimated to be 3.92×10^{-3} photons/cm^2. With a Fermi/GBM effective area of 322 cm^2 that would be a detection of 1.26 photons. The main beam TGF luminosity would only need to be brighter by one order of magnitude or 10^{18} photons > 1 MeV for the reverse beam to exceed the minimum detection threshold of the Fermi/GBM, which is 8 counts in the BGO detectors combined. This estimate takes into account both how much more penetrating the reverse beam is compared to the main beam as well as the larger relative signal due to its narrow beaming.

An alternative approach is to define a 'typical' upward TGF from Fermi/GBM observations and compare our simulation results to that as a standard candle. We start by defining our typical Fermi TGF as having a source altitude of 12 km, intensity on the order of 10^{17} photons >1 MeV, a median radial distance from the Fermi/GBM of 311 km (*GBM Terrestrial Gamma-ray Flashes (TGF) Catalog*, 2016), and having an average count of roughly 50 including both BGO detectors and the sum of the NaI detectors for TGF durations less than 200 μs (Briggs, 2013). The Monte Carlo Geant4 simulations, using our atmospheric model, of this typical TGF show a simulated fluence of 0.05 cm^{-2} at the typical 311 km annulus, consistent with previous analyses of typical orbital TGF fluence rates on the order of 0.1 cm^{-2} (Østgaard et al., 2012; Dwyer et al., 2017).

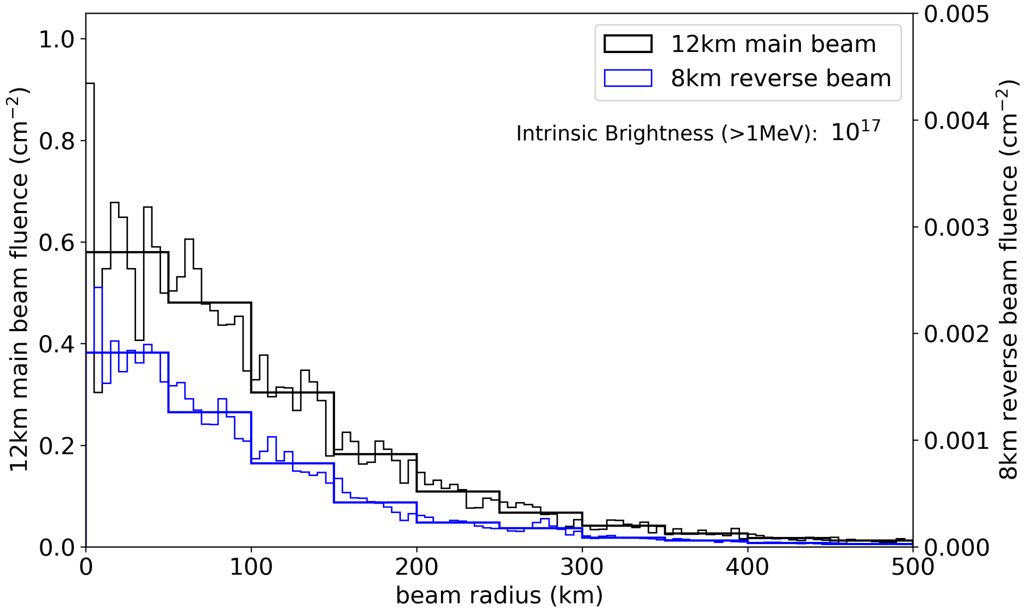

Figure 8. Black: Gamma ray fluence captured at 530 km from a 12 km upward TGF scaled to an intrinsic brightness of 10^{17} photons >1 MeV binned in both 5 km annuli and 50 km annuli. Blue: Gamma ray flux captured at 530 km from an 8 km reverse beam of a downward TGF scaled to an intrinsic brightness of 10^{17} photons >1 MeV binned in both 5 km annuli and 50 km annuli.

Using the fluence values from Figure 8 we can calculate the ratio between the 50 km beam center of an upward TGF with a 12 km source altitude (0.59) and the reverse beam of a downward TGF with an 8 km source altitude (0.0017) with the same intrinsic luminosity as roughly 0.59/0.0017 = 350. In other words, for the reverse beam TGF to attain an equivalent fluence within the center of the beam at orbital altitudes to a typical 12km upward TGF at beam center the 8km downward TGF would need to be 350 times brighter or 3×10^{19}, well beyond any previously published estimates of observed

TGF luminosity. However, the fluence of the upward 12km TGF at its 311 km annulus (.06) is only 35 times brighter than the reverse beam fluence at beam center of the 8km downward TGF (0.0017). Meaning, the 8 km downward TGF would need to be 35 times brighter for the reverse beam with optimal beaming angle to be observed by Fermi with a count rate typical of Fermi observations. Finally, the total counts for the 25 July event (8 BGO counts + 10 Nai counts) are roughly $\frac{2}{5}$ our definition of a typical Fermi TGF. A downward TGF at 8 km would only need to be $(35\times\frac{2}{5})$=14 times brighter than our defined typical upward TGF, giving a brightness estimate of 1.4×10^{18} at 8 km, consistent with our estimate of 2×10^{18} for a 7.5 km downward TGF.

7 Summary

The proposed scenario (Pu et al., 2020) of a bi-directional CG leader initiating at 6-7 km resulting in a downward directed TGF from an upward propagating positive leader, whose reverse beam component was observed by Fermi/GBM, seems likely. The estimated negative charge center altitude at 8 km is consistent with our best estimate of the source altitude of the TGF at 7.5 km. We have also shown, using Monte Carlo simulations, that the reverse beam of this TGF is detectable from orbit under ideal beaming conditions in large part due to the hardness of the reverse beam spectrum. Our estimate for the lower limit of intrinsic brightness of 2×10^{18} is bright, but not without precedent.

Acknowledgments

We would like to thank David Sarria of the Birkeland Centre for Space Science at the University of Bergen for a fruitful discussion and comparison of REAM/Geant4 particle simulation results. J. M. C., and D. M. S. acknowledge the support of the National Science Foundation award AGS-1935989. The code and data files used in this work are available online (https://doi.org/10.7291/D1GM4P).

References

Abbasi, et al. (2022). First high-speed camera observations of the optical counterpart of a terrestrial gamma-ray flash. *eprint arXiv:2205.05115*.

Abbasi, R. U., Abe, M., Abu-Zayyad, T., Allen, M., Anderson, R., Azuma, R., . . . Zundel, Z. (2017, August). The bursts of high energy events observed by the telescope array surface detector. *Physics Letters A*, *381*, 2565-2572. doi: 10.1016/j.physleta.2017.06.022

Abbasi, R. U., et al. (2018). Gamma-ray Showers Observed at Ground Level in Coincidence With Downward Lightning Leaders. *Journal of Geophysical Research (Atmospheres)*. doi: 10.1029/2017JD027931

Agostinelli, Allison, Amako, Apostolakis, Araujo, Arce, et al. (2003). Geant4 - a simulation toolkit. *Nuclear Instruments and Methods in Physics Research*. doi: 10.1016/S0168-9002(03)01368-8

Allison, Amako, Apostolakis, Araujo, Dubois, A., Asai, et al. (2006). Geant4 developments and applications. *IEEE Transactions on Nuclear Science*. doi: 10.1109/TNS.2006.869826

Allison, Amako, Apostolakis, Arce, Asai, Aso, et al. (2016). Recent developments in geant4. *Nuclear Instruments and Methods in Physics Research*. doi: 10.1016/j.nima.2016.06.125

Biagi, C. J., Uman, M. A., Hill, J. D., & Jordan, D. M. (2011). Observations of the initial, upward-propagating, positive leader steps in a rocket-and-wire triggered lightning discharge. *Geophysical Research Letters*. doi: https://doi.org/10.1029/2011GL049944

Bowers, G. S., Smith, D. M., Kelley, N. A., Martinez-McKinney, G. F., Cummer, S. A., Dwyer, J. R., . . . Rassoul, H. K. (2018). A Terrestrial Gamma-Ray

Flash inside the Eyewall of Hurricane Patricia. *J. Geophys. Res.*, *123*. doi: https://doi.org/10.1029/2017JD027771

Bowers, G. S., Smith, D. M., Martinez-McKinney, G. F., Kamogawa, M., Cummer, S. A., Dwyer, J. R., ... Kawasaki, Z. (2017, October). Gamma Ray Signatures of Neutrons From a Terrestrial Gamma Ray Flash. *Geophys. Res. Let.*, *44*, 10. doi: 10.1002/2017GL075071

Briggs, M. S., Xiong, S., Connaughton, V., Tierney, D., Fitzpatrick, G., Foley, S., ... Hutchins, M. L. (2013, June). Terrestrial gamma-ray flashes in the Fermi era: Improved observations and analysis methods. *Journal of Geophysical Research (Space Physics)*, *118*, 3805-3830. doi: 10.1002/jgra.50205

Cummer, S. A., Briggs, M. S., Dwyer, J. R., Xiong, S., Connaughton, V., Fishman, G. J., ... Solanki, R. (2014, December). The source altitude, electric current, and intrinsic brightness of terrestrial gamma ray flashes. *Geophys. Res. Let.*, *41*, 8586-8593. doi: 10.1002/2014GL062196

Cummer, S. A., Lu, G., Briggs, M. S., Connaughton, V., Xiong, S., Fishman, G. J., & Dwyer, J. R. (2011, July). The lightning-TGF relationship on microsecond timescales. *Geophys. Res. Let.*, *38*, 14810. doi: 10.1029/2011GL048099

Cummer, S. A., Zhai, Y., Hu, W., Smith, D. M., Lopez, L. I., & Stanley, M. A. (2005). Measurement and implications of the relationship between lightning and terrestrial gamma-ray flashes. *Geophys. Res. Let.*, *32*, L22804.

Dowell, D. C., Alexander, C. R., James, E. P., Weygandt, S. S., Benjamin, S. G., Manikin, G. S., ... Alcott, T. I. (2022). The high-resolution rapid refresh (hrrr): An hourly updating convection-allowing forecast model. part i: Motivation and system description. *AMS Journals*. doi: 10.1175/WAF-D-21-0151.1

Dwyer, & Cummer, S. A. (2013). Radio emissions from terrestrial gamma-ray flashes. *Journal of Geophysical Research: Space Physics*, 3769–3790. doi: 10.1002/jgra.50188

Dwyer, Liu, Grove, Rassoul, & Smith. (2017). Characterizing the source properites of terrestrial gamma ray flashes. *Journal of Geophysical Research (Space Physics)*, *122*, 8915-8932. doi: 10.1002/2017JA024141

Dwyer, J., Rassoul, H., Al-Dayeh, M., Caraway, L., Chrest, A., Wright, B., ... Rambo, K. (2005). X-ray bursts associated with leader steps in cloud-to-ground lightning. *Geophys. Res. Let.*, *32*, L01803. doi: 10.1029/2004GL021782

Dwyer, J., Smith, D., & Cummer, S. (2012). High−Energy Atmospheric Physics: Terrestrial Gamma-Ray Flashes and Related Phenomena. *Space Sci Rev*, *173*, 133–196. doi: 10.1007/s11214-012-9894-0

Dwyer, J. R. (2003a). A fundamental limit on electric fields in air. *Geophys. Res. Let.*, *30*(20), 2055.

Dwyer, J. R. (2007). Relativistic breakdown in planetary atmospheres. *Physics of Plasmas*, *14*, 042901. doi: 10.1063/1.2709652

Dwyer, J. R. (2021). Terrestrial gamma-ray flashes initiated by positive leaders. *Phys. Rev. D*, *104*.

Dwyer, J. R., Liu, N., Eric Grove, J., Rassoul, H., & Smith, D. M. (2017, August). Characterizing the source properties of terrestrial gamma ray flashes. *Journal of Geophysical Research (Space Physics)*, *122*, 8915-8932. doi: 10.1002/2017JA024141

Dwyer, J. R., Rassoul, H., Al-Dayeh, M., Caraway, L., Chrest, A., Wright, B., ... Smyth, C. (2004a). A ground level gamma-ray burst observed in association with rocket-triggered lightning. *Geophys. Res. Let.*, *31*, L05119. doi: 10.1029/2003GL018771

Dwyer, J. R., Rassoul, H., Al-Dayeh, M., Caraway, L., Chrest, A., Wright, B., ... Smyth, C. (2004b). Measurements of x-ray emission from rocket-triggered lightning. *Geophys. Res. Let.*, *31*, L05118. doi: 10.1029/2003GL018770

Dwyer, J. R., & Smith, D. M. (2005). A comparison between Monte Carlo simulations of runaway breakdown and terrestrial gamma-ray flash observations. *Geophys. Res. Let.*, *32*, L08811. doi: 10.1028/2005GL023848

Enoto, T., Wada, Y., Furuta, Y., Nakazawa, K., Yuasa, T., Okuda, K., . . . Tsuchiya, H. (2017, November). Photonuclear reactions triggered by lightning discharge. *Nature*, *551*, 481-484. doi: 10.1038/nature24630

GBM terrestrial gamma-ray flashes (TGF) catalog. (2016). Retrieved from `https://fermi.gsfc.nasa.gov/ssc/data/access/gbm/tgf/`

Gjesteland, T., Østgaard, N., Laviola, S., Miglietta, M. M., Arnone, E., Marisaldi, M., . . . Montanya, J. (2015, December). Observation of intrinsically bright terrestrial gamma ray flashes from the Mediterranean basin. *Journal of Geophysical Research (Atmospheres)*, *120*(D9), 12. doi: 10.1002/2015JD023704

Gurevich, Milikh, G. M., & Roussel-Dupré, R. A. (1992). Runaway electron mechanism of air breakdown and preconditioning during a thunderstorm. *Physics Letters A*, *165*, 463.

Gurevich, A., Carlson, H. C., Medvedev, Y. V., & Zybin, K. (2000). Generation of electron-positron pairs in runaway breakdown. *Phys. Lett.*, 101–108.

Hare, B. M., Uman, M. A., Dwyer, J. R., Jordan, D. M., Biggerstaff, M. I., Caicedo, J. A., . . . Bozarth, A. (2016, June). Ground-level observation of a terrestrial gamma ray flash initiated by a triggered lightning. *Journal of Geophysical Research (Atmospheres)*, *121*, 6511-6533. doi: 10.1002/2015JD024426

Jayaratne. (1983). Laboratory studies of the charging of soft-hail during ice crystal interactions. *Quarterly Journal of the Royal Meteorological Society*. doi: 10.1002/qj.49710946111

Kereszy, I., Rakov, V. A., Ding, Z., , & Dwyer, J. R. (2022). Ground-based observation of a tgf occurring between opposite polarity strokes of a bipolar cloud-to-ground lightning flash. *Journal of Geophysical Research: Atmospheres*, *127*. doi: e2021JD036130

Kotovsky, D. A., Uman, M. A., Wilkes, R. A., & Jordan, D. M. (2019). High-speed video and lightning mapping array observations of in-cloud lightning leaders and an m component to ground. *Journal of Geophysical Research: Atmospheres*. doi: https://doi.org/10.1029/2018JD029506

Lindanger, A., Marisaldi, M., Sarria, D., Østgaard, N., Lehtinen, N., Skeie, C. A., . . . Neubert, T. (2021). Spectral analysis of individual terrestrial gamma-ray flashes detected by ASIM. *Journal of Geophysical Research: Atmospheres*, *126*. doi: e2021JD035347

Lu, G., Blakeslee, R. J., Li, J., Smith, D. M., Shao, X.-M., McCaul, E. W., . . . Cummer, S. A. (2010). Lightning mapping observation of a terrestrial gamma-ray flash. *Geophys. Res. Let.*, *37*, L11806. doi: 10.1029/2010GL043494

Luque, M. Y., Nollas, F., Pereyra, R. G., Bürgesser, R. E., & Ávila, E. E. (2020). Charge separation in collisions between ice crystals and a spherical simulated graupel of centimeter size. *Journal of Geophysical Research: Atmospheres*. doi: https://doi.org/10.1029/2019JD030941

Lyu, F., Cummer, S. A., Briggs, M., Marisaldi, M., Blakeslee, R. J., Bruning, E., . . . Stanbro, M. (2016). Ground detection of terrestrial gamma ray flashes from distant radio signals. *Geophysical Research Letters*, 8728–8734. doi: 10.1002/2016GL070154

Lyu, F., Cummer, S. A., Krehbiel, P. R., Rison, W., Bruning, E. C., & Rutledge, S. A. (2021). A distinct class of high peak current lightning pulses over mountainous terrain in thunderstorms. *Geophysical Research Letters*. doi: 10.1029/2021GL094153

Lyu, F., Cummer, S. A., & McTague, L. (2015). Insights into high peak current in-cloud lightning events during thunderstorms. *Geophys. Res. Lett.*, 6836–6843. doi: 10.1002/2015GL065047

Mailyan, B. G., Briggs, M. S., Cramer, E. S., Fitzpatrick, G., Roberts, O. J., Stanbro, M., . . . Dwyer, J. R. (2016, November). The spectroscopy of individual terrestrial gamma-ray flashes: Constraining the source properties. *Journal of Geophysical Research (Space Physics)*, *121*(A10), 11. doi: 10.1002/2016JA022702

Marisaldi, M., Fuschino, F., Tavani, M., Dietrich, S., Price, C., Galli, M., ... Vercellone, S. (2014, February). Properties of terrestrial gamma ray flashes detected by AGILE MCAL below 30 MeV. *Journal of Geophysical Research (Space Physics)*, *119*, 1337-1355. doi: 10.1002/2013JA019301

Moore, C. B., Eack, K. B., Aulich, G. D., & Rison, W. (2001). Energetic radiation associated with lightning stepped-leaders. *Geophys. Res. Let.*, *28*(11), 2131-2144.

Ortberg, J., Smith, D. M., Li, J., Dwyer, J., & Bowers, G. (2020). Detecting an upward terrestrial gamma ray flash from its reverse positron beam. *JGR Atmospheres*. doi: 10.1029/2019JD030942

Østgaard, N., Gjesteland, T., Carlson, B. E., Collier, A. B., Cummer, S. A., Lu, G., & Christian, H. J. (2013). Simultaneous observations of optical lightning and terrestrial gamma ray flash from space. *Geophysical Research Letters*, *40*, 2423-2426. doi: 10.1002/grl.50466

Østgaard, N., Gjesteland, T., Hansen, R. S., Collier, A. B., & Carlson, B. (2012, March). The true fluence distribution of terrestrial gamma flashes at satellite altitude. *Journal of Geophysical Research (Space Physics)*, *117*, 3327. doi: 10.1029/2011JA017365

Pu, Y., Cummer, S. A., Huang, A., Briggs, M., Mailyan, B., & Lesage, S. (2020). A Satellite-Detected Terrestrial Gamma Ray Flash Produced by a Cloud-to-Ground Lightning Leader. *Geophysical Research Letters*, *47*. doi: 10.1029/2020GL089427

Pu, Y., Cummer, S. A., Lyu, F., Briggs, M., Mailyan, B., Stanbro, M., & Roberts, O. (2019). Low Frequency Radio Pulses Produced by Terrestrial Gamma-Ray Flashes. *Geophysical Research Letters*, *46*, 6990-6997. doi: 10.1029/2019GL082743

Smith, D. M., Bowers, G. S., Kamogawa, M., Wang, D., Ushio, T., Ortberg, J., ... Stock, M. (2018). Characterizing upward lightning with and without a terrestrial gamma ray flash. *Journal of Geophysical Research: Atmospheres*, *123*. doi: 10.1029/2018jd029105

Smith, D. M., Hazelton, B. J., Grefenstette, B. W., Dwyer, J. R., Holzworth, R. J., & Lay, E. H. (2010). Terrestrial gamma ray flashes correlated to storm phase and tropopause height. *J. Geophys. Res.*, *115*, A00E49. doi: 10.1029/2009JA014853

Smith, D. M., Kelley, N. A., Buzbee, P., Infanger, A., Splitt, M., Holzworth, R. H., & Dwyer, J. R. (2020). Special classes of terrestrial gamma ray flashes from rhessi. *JGR Atmospheres*, *125*. doi: 10.1029/2020JD033043

Stanley, M. A., Shao, X., Smith, D. M., Lopez, L., Pongratz, M., Harlin, J., ... Regan, A. (2006). A link between terrestrial gamma-ray flashes and intracloud lightning discharges. *Geophys. Res. Let.*, *33*, L06803. doi: 10.1029/20005GL025537

Takahashi. (1978). Riming electrification as a charge generation mechanism in thunderstorms. *Journal of the Atmospheric Sciences*. doi: 10.1175/1520-0469(1978)035⟨1536:REAACG⟩2.0.CO;2

Taranenko, T., & Roussel-Dupré, R. A. (1996). High altitude discharges and gamma-ray flashes: a manifestation of runaway air breakdown. *Geophys. Res. Let.*, *23*(5), 571-574.

Tierney, D., Briggs, M. S., Fitzpatrick, G., Chaplin, V. L., Foley, S., McBreen, S., ... Wilson-Hodge, C. (2013, October). Fluence distribution of terrestrial gamma ray flashes observed by the Fermi Gamma-ray Burst Monitor. *Journal of Geophysical Research (Space Physics)*, *118*, 6644-6650. doi: 10.1002/jgra.50580

Tran, et al. (2015). A terrestrial gamma-ray flash recorded at the Lightning Observatory in Gainesville, Florida. *Journal of Atmospheric and Solar-Terrestrial Physics*.

Wada, Y., Morimoto, T., Nakamura, Y., Wu, T., Enoto, T., Nakazawa, K., ... Tsuchiya, H. (2022). Characteristics of low-frequency pulses associated with downward terrestrial gamma-ray flashes. *Geophysical Research Letters*. doi: 10.1029/2021GL097348

Wang, Z., Qie, X., Jiang, R., Wang, C., Lu, G., Sun, Z., ... Pu, Y. (2016). High-speed video observation of stepwise propagation of a natural upward positive leader. *Journal of Geophysical Research: Atmospheres*. doi: https://doi.org/10.1002/2016JD025605

Zhu, Y., Rakov, V. A., & Tran, M. D. (2016). A study of preliminary breakdown and return stroke processes in high-intensity negative lightning discharges. *Atmosphere*, *130*. doi: https://doi.org/10.3390/atmos7100130